Crustal formation on a spreading ridge above a mantle plume: receiver function imaging of the Icelandic crust

J. Jenkins[1], J. Maclennan[2], R. G. Green[1], S. Cottaar[2], A. F. Deuss[3], R. S. White[2]

[1]GeoForschungsZentrum Potsdam, Potsdam, Germany
[2]Bullard Laboratories, University of Cambridge, UK
[3]University of Utrecht, Netherlands

Key Points:

- Seismic discontinuity structure of the Icelandic crust is imaged using RF and dispersion data
- We image a ≈20 km thick layer underlain by a lens of higher velocity material to depths of 44 km
- Structure may form via magmatic underplating or lateral variability in supplied melt composition

Corresponding author: J. Jenkins, `jjenkins@gfz-potsdam.de`

Abstract

Iceland sits astride a mid-ocean ridge underlain by a mantle hotspot. The interplay of these two geological processes has the potential to generate a complex and laterally variable crustal structure. The thickness of the Icelandic crust is a long running and controversial debate, with estimates ranging from a "thin" 20 km crust to a "thick" 40 km crust. We present new images of the first order seismic discontinuity structure of the Icelandic crust based on a joint inversion of receiver function and ambient noise derived surface wave dispersion data. Inversion results are validated through comparison to receiver functions multi-phase common conversion point stacks across the densely instrumented Northern Volcanic Zone. We find a multi-layered crustal structure consisting of a 6-10 km deep upper crust underlain by either one or two discontinuities. The shallower discontinuity is found at depths of ≈20 km throughout Iceland. The deeper discontinuity is only present in some regions, defining the base of a lens-like lower layer with maximum depths of 44 km above the center of the mantle plume. Either of these two discontinuities could be interpreted as the seismic Moho, providing an explanation why previous estimates of crustal thickness have diverged. Such structure may form via underplating of a pre-existing oceanic crust as has been hypothesized in other ocean island plume settings. However we demonstrate with a simple petrological model that variability in seismic discontinuity structure can also be understood as a consequence of compositional variation in melts generated with distance from the plume center.

1 Introduction

Iceland straddles the mid-Atlantic spreading ridge, where the separation of the North American and Eurasian plates leads to the formation of new oceanic crust. In addition, Iceland is also underlain by a hotspot, which is generally considered to be the surface expression of a deep sourced mantle plume [e.g *White and McKenzie*, 1989; *White*, 1997; *French and Romanowicz*, 2015; *Jenkins et al.*, 2016]. Crustal formation occurring today along Iceland's volcanic rift zones is generated through the interplay of two geological processes: decompression melting occurring in the core of the convecting mantle plume and decompression melting as a result of plate spreading. The extent of this interaction and the relative importance of each process has the potential to form a complex and laterally variable crustal structure.

The full plate spreading rate of 18.5 mm/yr in Iceland [MORVEL *DeMets et al.*, 2010] is accommodated across a series of offset segments defined by volcanic rift zones (Figure 1).

Active rifting is currently taking place along the Northern Volcanic Zone (NVZ) and on two sub-parallel rift zones in southern Iceland: the Western and Eastern Volcanic Zones (WVZ and EVZ), Figure 1. It is generally considered that the WVZ and EVZ are the result of a jump in active rifting moving eastwards, with the WVZ gradually dying out over time [*Einarsson*, 2008]. The locus of active rifting is thought to have moved eastwards in a series of rift jumps from the NW rift, to the Snæfellsnes-Húnaflói rift and finally to the present day active western and northern volcanic zones over the last 24 Ma [*Harðarson et al.*, 2008]. Such jumps are hypothesized to follow the location of the underlying mantle plume [*Saemundsson*, 1974], which is currently centered beneath Vatnajökull ice cap [*Shorttle et al.*, 2010].

Iceland's volcanic rift zones are delineated by elongate fissure swarms 5-20 km wide and 10s-100 km long, oriented approximately normal to the spreading direction. Individual segments are generally fed by a central volcano, with the majority of magmatic activity producing basaltic compositions [*Gudmundsson*, 2000].

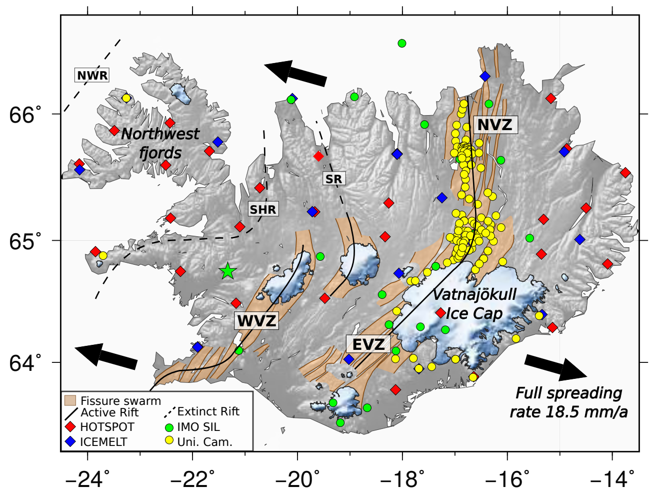

Figure 1. Map of seismic station distribution and key tectonic features discussed in this paper. Northern, Western and Eastern volcanic active rift zones are marked as NVZ, WVZ and EVZ respectively. Extinct rift zones are labeled as NWR Northwest, SHR - Snæfellsnes-Húnaflói and SR - Skagafjördur, locations based on *Harðarson et al.* [2008]. Plate spreading rates are from [MORVEL; *DeMets et al.*, 2010].

Since the first seismic measurements were made during the 1960s, the thickness of the Icelandic crust has been at the center of a long running and controversial debate. Though most studies have imaged similar crustal structure, the way such structure is interpreted leads to two very different models of the Icelandic crust. The earliest studies modeled a crust of approximately 10-20 km thickness underlain by an unusually low velocity mantle (Vp = 7.2 km/s) [e.g. *Pálmason*, 1971], interpreted as being partially molten [e.g. *Gebrande et al.*, 1980]. This is often called “layer 4” in the literature, referring to an additional layer beneath the 3-layered typical oceanic crustal structure (1. unconsolidated sediments, 2. basaltic pillow lavas underlain by dykes, 3. gabbros and ultramafic cumulates). Assuming layer 4 represents low-velocity mantle leads to the “thin” crustal model, and is supported by evidence of a layer of high electrical conductivity beneath ~20 km depth, interpreted as melt ponding beneath the Moho [*Beblo and Bjornsson*, 1980; *Hersir et al.*, 1984; *Eysteinsson and Hermance*, 1985]. Additional evidence comes from high surface heat flow measurements suggesting that basaltic material would be molten at depths greater than approximately 20 km [*Flóvenz and Saemundsson*, 1993].

From the 1990s onwards a series of refraction experiments in Iceland [*Menke et al.*, 1996; *Brandsdóttir et al.*, 1997; *Staples et al.*, 1997; *Menke et al.*, 1998; *Darbyshire et al.*, 1998; *Weir et al.*, 2001], observed reflected and refracted phases coming from depths of up to 40 km. These phases were interpreted as signals from the seismic Moho, leading to the “thick” crustal model. High Vp velocities of 7.2 km/s beneath 20 km depth in this model then represent an unusually high-velocity lower crust, which has been hypothesized to be formed of MgO rich compositions generated by high temperature melting in the mantle plume [*White and McKenzie*, 1989]. Observations of low attenuation factors at depth [*Menke and Levin*, 1994], and seismicity down to 12 km depth [*Stefánsson et al.*, 1993; *Menke and Sparks*, 1995], support this interpretation, arguing for a cold subsolidus lower crust, as opposed to a partially molten upper mantle. More recent studies now tend to favor the thick crust model [e.g *Darbyshire et al.*, 2000; *Kaban et al.*, 2002; *Allen et al.*, 2002]. See *Brandsdóttir and Menke* [2008] for an in-depth review of the thin/thick crust debate.

Here we revisit the question of Icelandic crustal velocity structure using a wealth of new data, sourced mainly from the University of Cambridge Icelandic seismic network and data shared by the Iceland Meteorological Office (IMO). Ps converted phases and receiver functions are analyzed in conjunction with the recent surface wave dispersion measurements derived from ambient noise by *Green et al.* [2017]. In this paper, seismic data are interrogated with two independent methods, the results of which are used to validate each other. This provides us with a new image of the first order seismic discontinuity structure and its lateral variability within the Icelandic crust. We then carry out some simple petrological modeling to demonstrate that the discontinuity structure we observe can be explained by melt source variability with distance from the plume center.

2 Seismic Data and Methods

2.1 Seismic stations and events

Seismic data are sourced from 160 stations in total, made up of networks distributed throughout Iceland (Figure 1). This includes the Global Seismic Network station BORG and nationally distributed temporary networks ICEMELT (17 instruments deployed between 1993−96 *Bjarnason et al.* [1996]) and HOTSPOT (28 instruments deployed between 1996−98 *Foulger et al.* [2000]). This is augmented by data from 38 stations running for varied periods between 1995−2017 supplied by the Icelandic Meteorological office (IMO−SIL network), and an additional 94 stations from the University of Cambridge seismic network (running for varied periods between 2008−2017), which is mainly located along the NVZ, providing a region of dense data coverage throughout a location of present day rifting.

Global events with magnitudes Mw between 6 and 8.5 occurring during the recording period of the instruments (up to September 2016), at epicentral distances of 30−90° are selected for receiver function analysis. This distance range restricts interference from upper mantle triplications at $< 30°$, and core interactions at $> 90°$.

2.1.1 Crustal Receiver Functions

We use the receiver function (RF) technique to image sharp changes in seismic velocity within the Icelandic crust. When steeply incident direct compressional (P) wave energy from an earthquake source hits a sharp change in seismic velocity (such as the seismic Moho), some of the energy is converted to shear (S) wave energy, setting up secondary P to S converted phases. In crustal studies the main phases of interest are direct Ps conversions as well as three major crustal multiples which reverberate in the crust before arriving at the recording station: the positive polarity PpPs phase and the negative polarity co-arriving PsPs+PpSs phases (Figure 2a).

P phases are recorded preferentially on the vertical component of motion while converted phases are preferentially recorded on horizontal components. By deconvolving the vertical from the horizontal components we remove the source time function, instrument response and source side effects, producing receiver functions (RFs), which contain peaks

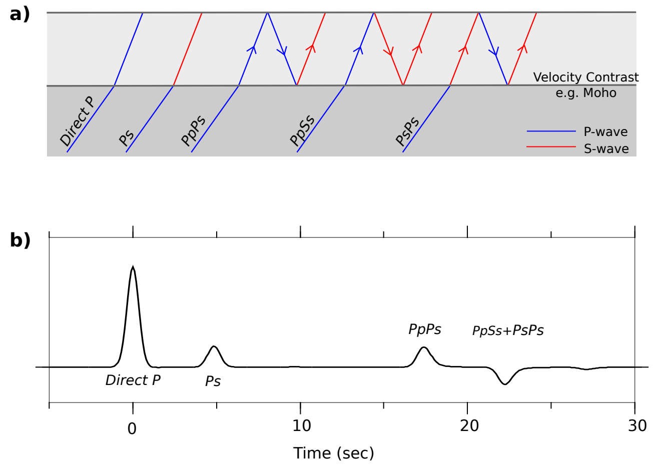

Figure 2. **a**) Ray paths of phases imaged in crustal RFs. **b**) Synthetic radial RF built with Gaussian pulses of width 2 s, for a simple crustal model with a 40 km deep Moho. Direct P arrival in addition to the Ps Moho converted phase and major crustal multiples are labeled.

representing Ps converted phase arrivals (Figure 2b). We produce RFs via the time domain iterative deconvolution method of *Ligorría and Ammon* [1999], building the RF with Gaussian pulses of a defined width varying from 2.0 to 0.5 s depending on the analysis approach and frequency content required. RFs are quality controlled based on reproduction tolerance of >70% (i.e. how well re-convolution of the RF and the vertical component can reproduce the horizontal components), the amplitude ratio of direct P amplitude to later arrivals, and visual inspection.

2.1.2 Surface wave dispersion

Rayleigh wave group velocity maps are generated using ambient noise analysis of the same seismic datasets. Fundamental mode surface wave signals are extracted through cross-correlation of the broadband seismic records between pairs of stations, and the group velocity dispersion is measured using Frequency Time Analysis (FTAN). Errors are parameterized based on the temporal repeatability of the dispersion measurements. Ray-path averaged inter-station velocity measurements are then tomographically inverted to calculate maps of the group velocity, which are well constrained at periods between 5-16 s (see *Green et al.* [2017] for more details). These periods have a sensitivity to shear velocity in the depths range of 0-25 km, with greatest sensitivity to shallower depths of < 15 km (see supplementary Figure

S1). We then sample each of the group velocity maps at station locations to extract dispersion curves for joint inversion with the RF at each station.

2.2 Methods Overview

We employ two independent methods to analyze our RF dataset with the aim of defining the seismic discontinuity structure of the Icelandic crust. Methods are summarized below, and discussed in detail in subsequent sections.

1. A joint inversion of RF and surface wave data is used to define the seismic velocity structure at each seismic station. The inversion is applied using a finely parameterized layer model (section 2.2.1) and a simplified coarse parameterized model guided by the results of the fine parameterization (section 2.2.2). Station point measurements are then interpolated to produce an island-wide model of seismic discontinuity structure.
2. RFs are stacked by their common conversion points (CCP) in the densely sampled NVZ. The presence of multiples is accounted for by migrating and stacking RFs using a multi-phase approach. Inversion model results are then validated by comparison with CCP stacks (sections 2.2.3 and 2.2.4).
3. Seismically imaged structure is then compared to petrological models of crustal structure produced by different melt compositions, via calculation of crystallization paths using MELTS software [*Ghiorso and Sack*, 1995] (methodological details can be found in the Petrological Modeling Section 4).

2.2.1 Joint inversion

RF and dispersion measurements have different and complementary sensitivities to crustal structure. RFs are sensitive to sharp velocity gradients which create converted phases, but are insensitive to absolute velocity structure. Surface wave dispersion curves in contrast are sensitive to absolute velocity, but are averaged over a wide depth range dependent on the period of observations, and are therefore insensitive to sharp gradients. Thus jointly inverting RF and surface wave dispersion data provides sensitivity to both sharp gradients and absolute velocities.

Here we use the inversion strategy of *Herrmann* [2013], as described in detail by *Julia et al.* [2000]. The method employs a simple damped least squares approach to iteratively update a defined starting model.

At each station, RFs built with a Gaussian pulse of 1 s are split into subsets of data from similar back-azimuths (BAZ) constrained by data distribution and waveforms similarity into bins of varying BAZ width (example in supplementary Figure S2), an approach advocated by previous studies [e.g. *Schlindwein*, 2006]. Typically this forms a collection of 1 to 7 subsets per station, each containing 3-18 highly similar waveforms. RFs in subsets are not stacked, but are instead considered as separate data pieces in the inversion, taking into account variations in waveforms expected for different epicentral distances. Corresponding dispersion measurements are extracted from tomographic fundamental mode Rayleigh wave group velocity maps of *Green et al.* [2017], with periods of 4-18 s. Accordingly each station will have several velocity models allowing for possible structural variations with BAZ.

The RF and dispersion data are weighted according to 3:1 = RF : dispersion data (see Supplementary Text S1 for discussion of how weighting and other variables affect inversion results [*Harmon and Rychert*, 2016]). Models are initially parameterized in 50 steps of 1 km above a constant half-space, and are run over 300 iterations. We use half-space starting models to remove any potential source of bias in inversion results from *a priori* assumptions of crustal structure. Inversions are run for 12 different half-space starting models with constant starting Vs ranging from 3.7 to 4.8 km/s. The resulting crustal models are compared and the average inversion result of all starting models is taken as the final model.

Finally, the resulting models are visually inspected, defining reliable results based on the following criteria:

1. the final fit to RF and surface wave data is > 60%
2. models converge to a constant value of data fit (as defined in [*Julia et al.*, 2000])
3. models converge to a similar solution from all 12 half-space starting models
4. models based on different data subsets show reasonably consistent results across back azimuths (BAZ) at a single station

After quality checks this leaves 800 station-BAZ inversion model results to be analyzed.

2.2.2 Simplified model parameterization

We then reduce the number of parameterized layers in inversion models to produce the simplest model possible required to fit major features in our seismic data. This allows us to identify robust major increases in velocity with depth, with the aim of defining the seismic Moho and crustal thickness.

An automated procedure is set up for the large dataset, guided by the initial inversion results from the finely parameterized 50-layer models. Finely parameterized inversion results show sharp gradients in the top 5-10 km before changing to a smoothly varying lower gradient velocity profile. Therefore, our simplified model parameterization allows a finely parameterized upper crust in 1 km steps down to the base of the observed high gradient region. Below this, one additional interface is imposed at depths varying from 15-45 km. The interface depth producing the greatest improvement to fit is selected as the best fitting model.

In many cases, we find that only one depth of interface in the 15-45 km depth range is suffcient to generate a peak in data fit. However, in some cases, inversion results indicate two potential discontinuity depths which both improve the data fit (see examples in Supplementary Figure S6). In such scenarios we allow a second interface to be added to the model parameterization. A large suite of model parameterizations are then generated to methodically test which combination of the two interface depths produces the maximum improvement to data fit. We then accept this 2-discontinuity model parameterization over a 1-discontinuity parameterization if both the misfit and the Akaike Information Criterion [*Akaike*, 1974] is reduced (examples in Supplementary Figure S8 and further details of methodology in Text S2).

2.2.3 Multi-phase time-depth conversion

RF peaks are generally converted from time to depth using a known velocity model under the assumption that peaks represent Ps converted phase arrivals. However, when analyzing shallow structure, converted phases and crustal multiples arrive at similar times, such that each arrival has the potential to be either a direct conversion or a multiple. Peaks which represent multiple phase arrivals will thus be migrated to incorrect depths in time-depth conversions. We combat this problem by applying multi-phase time-depth conversions, similar to those used by *Kind et al.* [2002], *Nábělek et al.* [2009] and *Tauzin et al.* [2016].

Each peak in the RF is converted from time to depth with the assumption that it is one of the following phases: Ps / PpPs / PpSs+PsPs. If the peak being migrated *is* the phase assumed, it will be migrated to the correct depth. Peaks representing other phases will be migrated to incorrect depths. Since a given discontinuity will create all 3 of the assumed phases, a peak representing each of the 3 phases is expected to be migrated to the true discontinuity depth in each of the different time-depth converted RFs, as shown in Figure 3a.

Since different time-depth conversions act to "stretch" RFs to different degrees, RFs are built with Gaussian pulses of the appropriate width such that they appear as a common wavelength after depth conversion (Figure 3b). RFs from different depth conversions can then be stacked together to bring out coherent signals. Only signals that are coherent between all depth conversions are stacked (taking into account the opposite polarity of PpSs+PsPs phases), before a moving average smoothing is applied to the final stack (Figure 3c).

In this study we have found that a Gaussian pulse width of 0.5 s for Pds (which equates to PpPs and PpSs widths of 2 s) gives an optimum balance between vertical resolution (5 km) and filtering of high frequency noise. In our data, signals generated by complex upper crustal structure often interfere with the earliest arriving direct Ps phases. Thus, while we perform all three depth conversions for visual inspection, combined stacks are generated using only the two multiple time-depth converted RFs.

We convert from time to depth assuming a 1D average shear wave velocity model, generated by averaging all of our 50-layer inversions results (see Supplementary Figure S14). We assume the depth dependent Vp/Vs relationship of *Allen et al.* [2002], to generate a corresponding P wave velocity profile.

2.2.4 Common Conversion Point stacking

We enhance the individual phase arrivals and suppress incoherent noise by stacking RFs with common conversion points (CCP) [*Dueker and Sheehan*, 1997; *Lekic et al.*, 2011]. A gridded volume stack is set up in the densely sampled NVZ region where there are many overlapping raypaths (Figure 4). The volume is defined as a region 130 km east-west by 190 km north-south about an origin at 64.5N, -18W, which is laterally sampled every 1 km^2 and vertically sampled every 0.1 km. RF raypaths (corresponding to the phase assumed in the time-depth conversion) are traced back through this volume, and the RF amplitude at depth is added to all points within two Fresnel zone radii of the ray (see Supplementary Text S3 for further details of stacking methodology). CCP stacking is also used to combine velocity profiles generated by inversions at individual stations. The resulting velocity profile is migrated back to depth along the raypaths of the RF used in the inversion, allowing direct comparison of inversion models and depth converted RF CCP stacks.

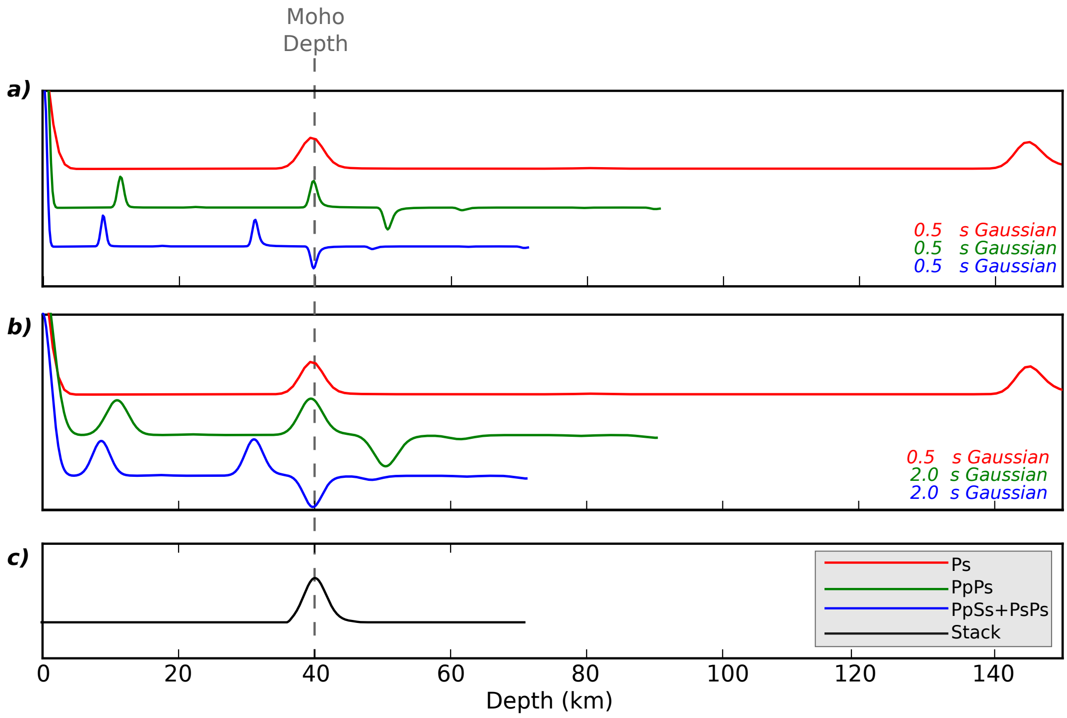

Figure 3. **a**) Synthetic RFs generated for a 40 km thick crust in a common frequency band, depth converted assuming peaks represent Pds phases (red), PpPs multiples (green) and PsPs+PpSs multiples (blue). **b**) RF depth converted in a similar fashion as in a, but built in 3 different frequency bands (as labeled). **c**) Stacked and smoothed time series of the three depth converted RFs shown in b. Dashed line shows true Moho depth.

3 Results

3.1 Joint inversion fine parameterization – general structure

An example of a typical inversion result is shown in Figure 5. From the surface to depths of 5-10 km the velocity gradient is high. We refer to this high-gradient region as the upper crust. Beneath this lies an abrupt transition to lower velocity-gradients, with velocities of a near constant value, showing only minor variations. At a depth of 20-25 km a sharp increase in velocity is often observed, followed by a return to near constant velocities, showing only minor variations with depth.

Results from all 12 half-space starting models (Figure 5a) converge to consistent solutions in the upper crust down to depths of approximately 15 km, due to constraints on absolute velocity from surface wave data (Figure 5b). Velocity variability between different starting models increases with depth below 15 km, since this region is beneath the depth res-

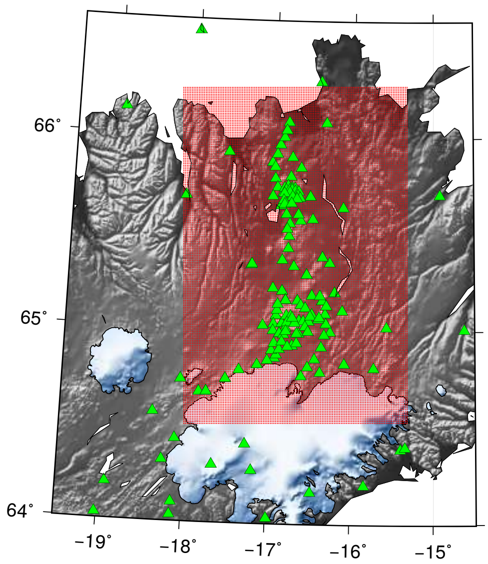

Figure 4. Definition of crustal multi-phase CCP stacking region over the NVZ. Seismic stations are shown as green triangles and finely spaced grid points are shown in red.

olution of dispersion data. Despite uncertainty in the absolute velocity at depth the general shape of the velocity profiles is consistent, and is independent of the starting model. Therefore we trust the first derivative of velocity dV/dZ, but not the absolute velocity of the inversion results at depths below 15 km. Tests show that the inversion results have little sensitivity to the choice of Vp/Vs ratio, the empirical density relation [*Berteussen*, 1977; *Carlson and Herrick*, 1990] or the use of realistic as opposed to half-space starting models (see Supplementary Text S1).

3.2 Joint inversion simplified model parameterization – maps

We then parameterize models with a finely layered upper crust underlain by either one or two interfaces (examples shown in Figure 5c), as required by data as described in section 2.2.2. Figure 6 shows the lateral distribution of stations suggesting either one or two major interfaces.

Single interface models require a best fitting layer at depths of 15-30 km with a peak in depths at ≈20 km. A similar depth range is reflected in the shallower of the double interface models, which we interpret as a continuation of the same interface. The deeper interface in the double interface models shows more variable depths ranging from 25-44 km below the surface.

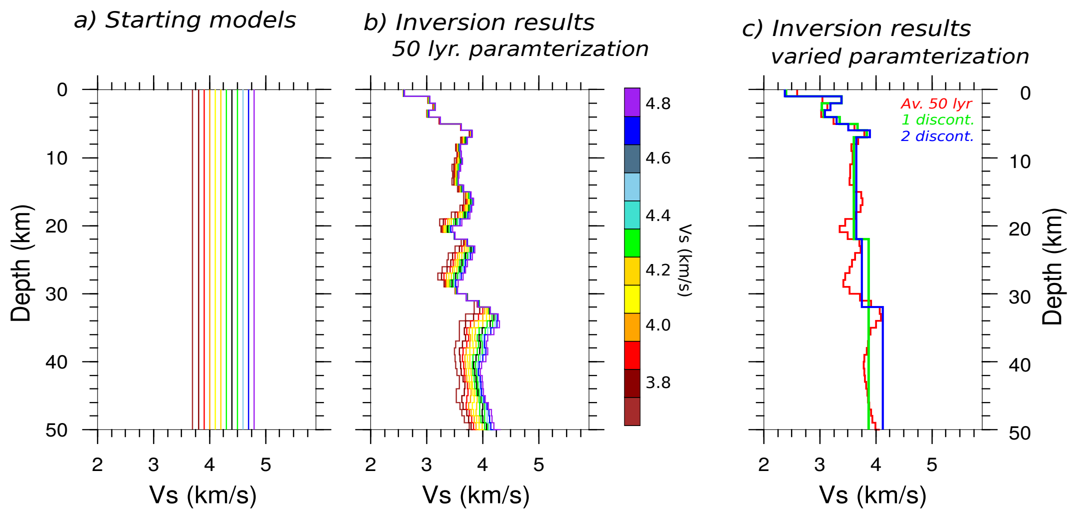

Figure 5. **a**) A range of half-space starting models with varying absolute velocities denoted by colors on scale to right; **b**) corresponding inversion results for station KSK located at 64.16N, -16.47W). **c**) Average of all 50-layer inversion results (red) compared to best fitting models found for a simplified model parameterization allow one additional discontinuity (green) and two additional discontinuities (green) beneath a finely parameterized upper crust.

The lateral distribution of where data requires a single or double interface model parameterization suggests that a two-layered deep crustal structure is only present in some parts of the Icelandic crust. Working on the assumption of a two-layered crust we divide our simple model parameterized results into two subsets. Models with a single interface are grouped with the shallower of the interfaces required in double interface models. A second group consists of single interface depths and the deeper of the double interface observations. These data points (shown in Figure 7 as points and interpolated surfaces), describe two discontinuities which will be referred to as A and B respectively.

Discontinuity A appears at near constant depths of ~20 km across Iceland, with deepening up to 30 km depth towards the north of Vatnajökull Icecap (Figure 7a). This layer is ~10-15 km shallower than previously predicted crustal thicknesses in this region [*Darbyshire et al.*, 2000; *Allen et al.*, 2002]. Extrapolation of discontinuity B data points produces a depth map which looks highly similar to maps of crustal thickness produced by previous studies of Icelandic crustal structure [*Darbyshire et al.*, 2000; *Allen et al.*, 2002] (Figure 7b).

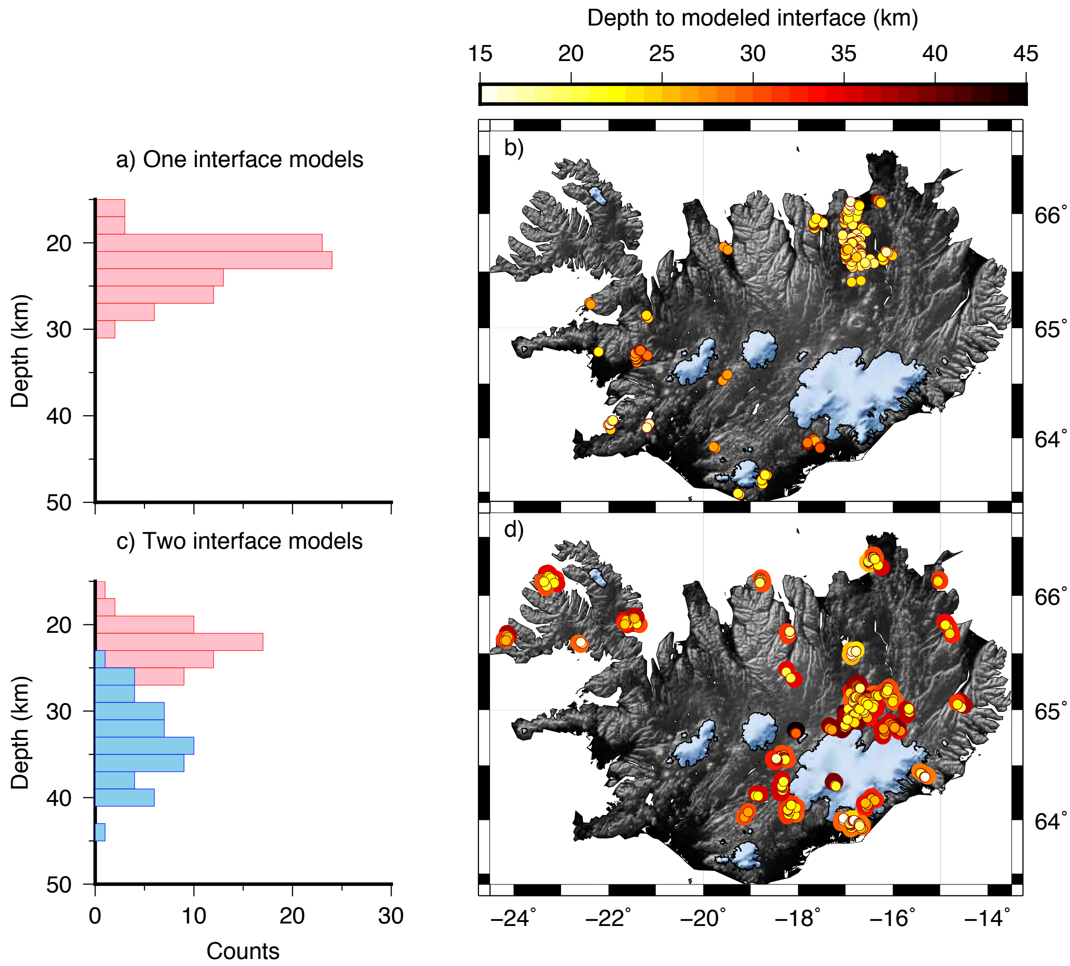

311 **Figure 6.** **a**) Results of simple inversion parameterizations, requiring either one (**a** and **b**) or two (**c** and **d**) interfaces below the finely parameterized 15 km thick upper crust. Results are shown as histograms of interface depth (**a** and **c**) and as maps with points colored as a function of depth (**b** and **d**). Double interface histogram **c**) show deeper interfaces in blue and shallower interfaces in pink, while the double interface model map **d**) shows deeper interfaces as larger points plotted behind shallower interfaces

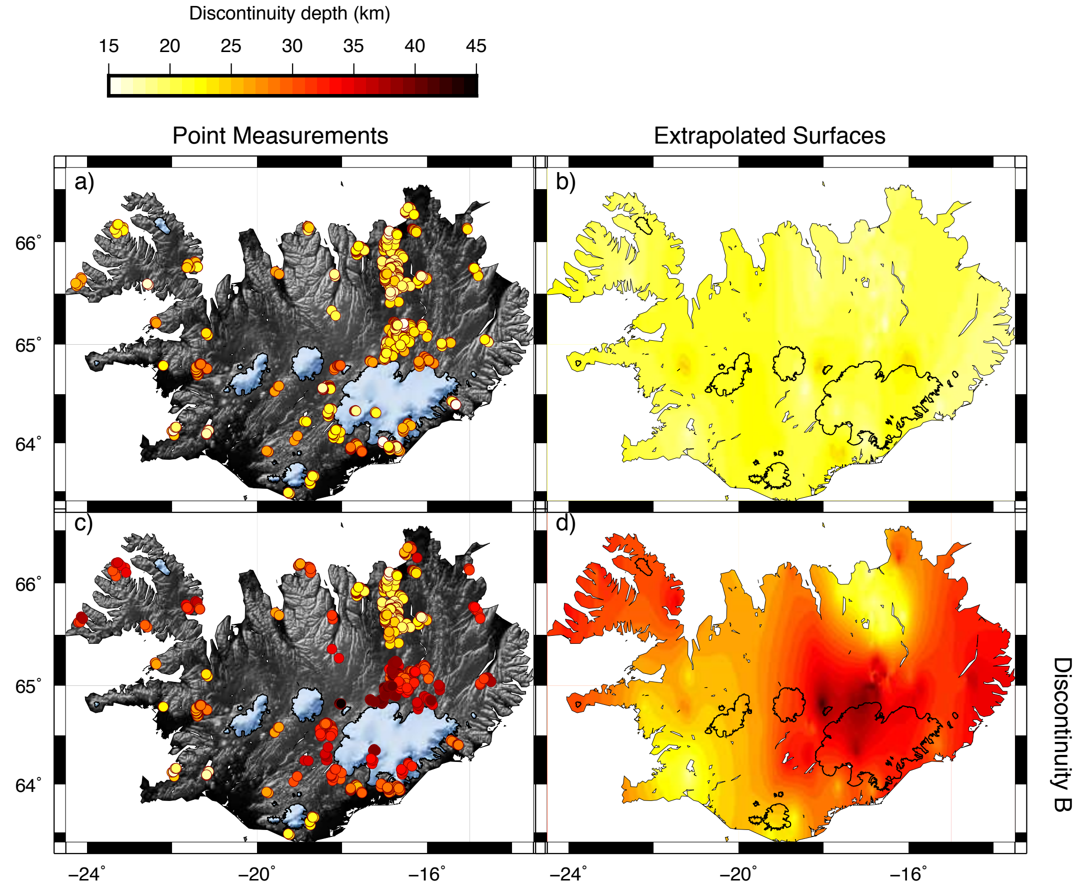

Figure 7. Map of forward modeled layer depths grouped into two discontinuities A and B. Left panels show the point measurements of discontinuity A (top), and discontinuity B (bottom). Right panels show depths of extrapolated surfaces through these points.

Cross-sections cut through discontinuity A and B surfaces (Figure 8), reveal that discontinuity B defines the base of a lens-like layer only present in specific regions, which have previously been interpreted as having large crustal thicknesses.

3.3 Common Conversion Point Stacks: Validation of Inversion results

To validate the existence of two major discontinuities as suggested by our inversion results, we directly compare CCP stacks of both time-to-depth converted RFs and velocity profiles derived from inversion. Figure 9 shows cross-sections through a region of the densely sampled NVZ region (location shown in Figure 9a), where inversion results predict the discontinuity structure to show the greatest range of observations (Figure 9c).

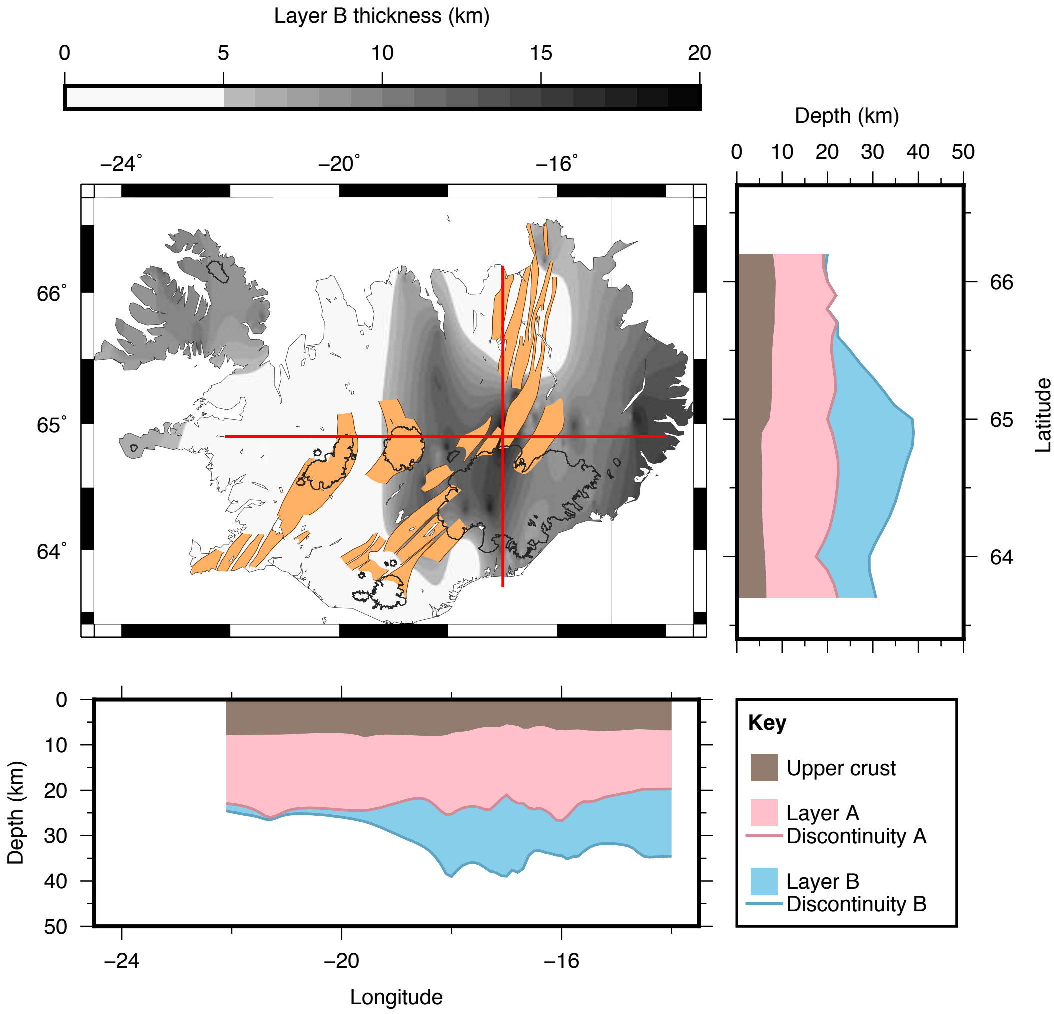

336 **Figure 8.** Cross section through extrapolated surfaces of discontinuities A and B shown in Figure 7. Central map shows differential thickness of discontinuities A and B with position of cross-sections marked by red lines. Volcanic fissure swarms are shown in orange.

Figure 9d shows that both of the two major discontinuities identified in simplified inversion parameterizations are clearly seen in time-depth migrated RF CCP stacks. CCP stacks of joint 50 layered inversion velocity results are shown in Figure 9e. Discontinuity A is observable in the velocity stack as a sharp increase to higher velocities, though discontinuity B is less clear.

As previously noted, the absolute velocities below ≈15 km are uncertain as the constraints from the dispersion data decrease strongly. However RFs still provide good resolution on the velocity gradients (dV/dZ). We show a stack of the velocity gradient in Figure 9f. Such a profile can be considered as a “pseudo RF” where the presence of multiples has already been accounted for, and each peak represents a sharp change in velocity, marked by an increase or decrease in velocity-gradient. Discontinuity A is clearly seen in Figure 9f, usually associated with the largest amplitude positive gradient peak. Deeper structure is more complex, but considering the results of simplified model inversion results and time-depth RF stacks a dipping layer consistent with discontinuity B can be identified within the dV/dZ stack.

Picked peaks representing each discontinuity in both time-depth and dV/dZ CCP stacks, show good similarity to our forward modeling results (Figure 9c), giving us confidence in the validity of the inversion results across Iceland from a simple parameterization. For further discussion of CCP results as well as maps of discontinuity depths derived from CCP stacks, see Supplementary Figure S13 and Text S4.

We note that discontinuity A appears to represent both a larger and a sharper increase in velocity with depth than discontinuity B. This is based on discontinuity A showing larger amplitude phase arrivals in depth RF stacks (indicating a larger velocity contrast across the boundary), and a large gradient peak in dV/dZ stacks (suggesting higher velocity-gradients and thus a sharper boundary).

Stacks are built using RFs time-depth converted using a velocity model constructed by averaging all inversion model results (as described in section 2.2.4). We find that using this velocity model significantly increases the signal coherency in stacked data compared to converting to depth assuming a constant average crustal velocity. However, discontinuity depths observed in CCP stacks built using these two different velocity models vary on average by only ±2 km. Therefore we assume that the choice of velocity model makes little significant difference to our first order results. See Supplementary Text S5 for details.

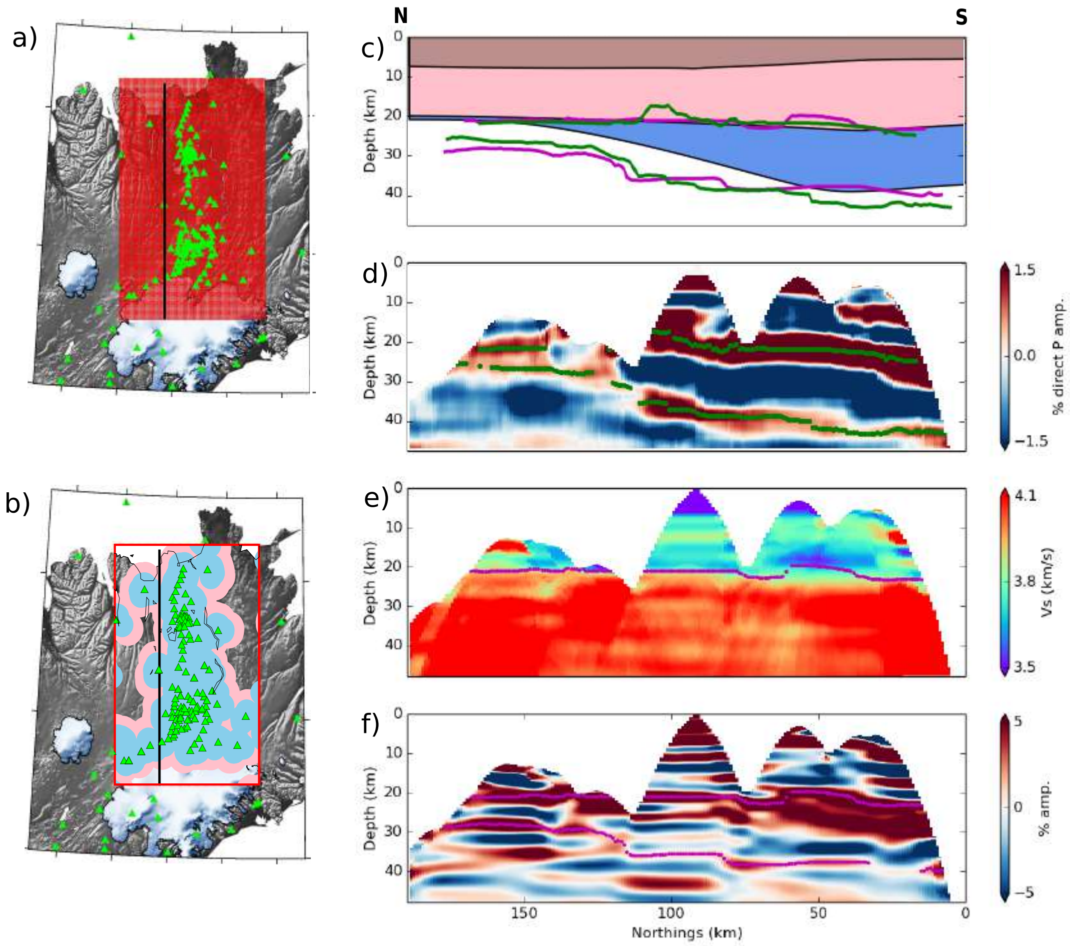

370 **Figure 9.** North-South cross-sections though CCP stacks along the NVZ. **a**) black line shows the location of plotted cross-sections, other features as labeled in Figure 4; **b**) shows data coverage as pierce points with a width of 2 times the fresenel zone at depths of 20 km (blue) and 40 km (pink). Cross-sections show **c**) interpreted structure from simplified model parameterization inversion results; **d**) depth converted RF; **e**) velocity structure from finely parameterized inversion results; **e**) first derivative dV/dZ of finely parameterized inversion results. Amplitude maxima picked peaks defining discontinuities A and B are shown for depth converted RF (green points in **d**) and dV/dZ stacks (magenta points in **f**), and compared to simple inversion modeled results in **b**.

4 Petrological Modeling - Seismic consequences of petrological variation across Iceland

Our seismic observations reveal a laterally variable crustal structure consisting of either one or two major crustal discontinuities. The discontinuities describe one layer of relatively consistent thickness, underlain by a lens-like layer of deeper material present only in certain regions, with greatest thicknesses above the center of the Iceland mantle plume (which lies beneath Vatnajökull ice cap). Here we explore whether our seismic observations can be reproduced by a petrological model which accounts for variability in melt sources in regions of crustal production.

4.1 Melt composition variability across Iceland

It is well-established that the variation in the Icelandic crust is linked to variations in the mean composition of the mantle melt being supplied under each volcanic system. For example, the northern part of the NVZ has an average erupted basalt composition that is relatively depleted in incompatible trace elements when compared with the more enriched basalts of the southern part of the NVZ (central Iceland) [*Maclennan et al.*, 2001a]. The coupled increase in crustal thickness (both interpreted by previous studies and observed here in the presence and thickness of layer B) and the increase in concentration of incompatible elements seen in the southern NVZ is likely to reflect the role of plume-driven upwelling in the generation of melts by adiabatic decompression of the mantle under central Iceland [*Maclennan et al.*, 2001a]. In contrast, melt generation under the northern NVZ can be accounted for by passive, plate-driven upwelling alone. While the mean composition of the melts generated under the rift zones varies significantly over length-scales of 10s–100s of km distance from the center of Iceland, it is also known that substantial compositional variability is present on a length-scale smaller than individual volcanic systems [*Slater et al.*, 2001; *Maclennan*, 2008; *Shorttle et al.*, 2010]. Both depleted and enriched mantle melts are supplied to the base of the crust of single volcanic systems across the Icelandic rift zones [*Maclennan*, 2008; *Rudge et al.*, 2013]. The fact that such compositional diversity is preserved in the extruded volcanic rocks indicates that mixing of diverse mantle melts is not complete prior to the onset of crystallization in magma chambers: depleted and enriched melts are present in close proximity in the crust of the rift zones.

The mantle melts under Iceland vary not only in their trace element composition but also in their major element contents. Trace element-enriched mantle melts generated under the rift zones are richer in iron but poorer in silicon and calcium than their depleted counterparts [*Shorttle and Maclennan*, 2011]. These differences in major element composition have important consequences for the evolution of melts during cooling in rift-zone magma bodies. When Icelandic mantle melts rise and cool they first start to crystallize olivine (i.e. olivine is the first phase on the liquidus) and then, after some further cooling, clinopyroxene and plagioclase join olivine in the assemblage of crystallizing solids. For example, *Winpenny and Maclennan* [2011] demonstrated that enriched melts have a much longer interval of cooling with olivine crystallization alone than do the depleted melts.

The significance of this petrological behavior for understanding the seismic structure of the Icelandic crust becomes clear when the properties of the solid rocks generated during cooling and fractional crystallization are considered. The olivine-rich ultramafic cumulates generated in the early stages of crystallization of mantle melts have physical properties that are similar to mantle rocks, with $V_p \sim 7.8$ km/s in the hot lower crust of Iceland [*Maclennan et al.*, 2001b]. At lower temperatures, plagioclase and clinopyroxene join the crystallizing assemblage and cumulate gabbro is the solid product. This gabbroic material has much lower seismic velocities than the ultramafic cumulates, with $V_p \sim 7.0$ km/s under lower crustal conditions [*Maclennan et al.*, 2001b]. Combining this understanding of the seismic properties of the cumulate rocks generated by crystallization, the differing crystallization paths of enriched and depleted mantle melts and the variation in the mean composition of mantle melts supplied across the rift zones of Iceland may provide a means of interpreting the seismic discontinuity structure displayed on Figures 7–11.

4.2 Petrological modeling of crystallization paths

We use simplified models of magmatic evolution and crustal accretion under Iceland's rift zones to explore this conceptual link. In order to capture the compositional variation with distance from the plume center we first assume that the ~20 km thick crust under the northern NVZ is generated by solidification of depleted mantle melts only, while the ~40 km thick crust of central Iceland is solidified from equal proportions of depleted and enriched mantle melts.

By using a bimodal distribution of melts we have made the simplification of assuming that only two melt compositions are supplied from the mantle and that no mixing takes place between these end-member melts or their derivatives. While these assumptions are not correct [*Maclennan*, 2008b], they are unlikely to invalidate our approach for the following reasons. First, the distribution of initial mantle melt compositions appears to be approximately bimodal [*Shorttle and Maclennan*, 2011]. Second, the importance of mixing in controlling compositional diversity is known to vary as a function of cooling, and relatively hot (MgO > 8.5 wt%) liquids preserve much of the initial compositional diversity inherited from the mantle melts [*Shorttle et al.*, 2016]. Third, petrological barometry indicates that substantial mixing takes place at depths of ≈15-20 km and shallower [*Maclennan*, 2008b]: the seismic discontinuities A and B are found at greater depths than this. We therefore investigate the generation of these discontinuities under the assumption that no mixing of end-member mantle melts takes place.

The major element compositions of depleted and enriched mantle melts are taken from *Shorttle and Maclennan* [2011], with both corrected to be in equilibrium with Fo_{90} olivine [*Danyushevsky and Plechov*, 2011] (for full details of compositions used in modelling please see Table S2 in the Supplementary Material). The crystallization paths of depleted and enriched mantle melts are modeled using the MELTS software with the ALPHAMELTS front-end [*Ghiorso and Sack*, 1995; *Smith and Asimow*, 2005]. In order to simplify these calculations, we assume that no mixing between depleted and enriched melts took place and that crystallization was fractional and isobaric at 5 kbar. The flexibility of ALPHAMELTS allows mixing and polybaric crystallization to be included in the models, but, as can be seen below, these relatively simple models provide an adequate description of the key first-order observations of seismic layering identified under Iceland. The MELTS calculations provide a great deal of information about the variation in the mineralogical, compositional and thermodynamic properties of the system as cooling takes place. The key results of interest here are the relationship between the temperature and the extent of crystallization (or percent of original liquid mass remaining) and the temperature/melt fraction at which the solidifying assemblage switches from olivine-dominated ultramafic cumulates to gabbros.

4.3 Crystallization paths for enriched and depleted melt sources

The relationship between mass percentage of the original mantle liquid and crystallization temperature for depleted melts is shown in Figure 10a. The onset of crystallization is at 1272°C, where the melt hits its liquidus at 100% liquid remaining. Olivine is the only crystallizing phase until about 1211°C after 6% mass loss to solids through fractional crystallization. Below this temperature, plagioclase and clinopyroxene join the crystallizing assemblage, such that the solid rock being generated is a gabbroic cumulate. Note the large change in gradient at the point where gabbroic crystallization starts, indicating that the mass generation of solid per unit cooling is much larger once gabbro is being generated. It has previously been demonstrated that crustal accretion of the middle and lower crust under Krafla and Theisterykir in the northern NVZ is well-described by a stacked-sills mode of accretion [*Kelemen et al.*, 1997; *Maclennan et al.*, 2001b]. In this model, solid material is added to the crust through fractional crystallization uniformly with depth and therefore the relationship between depth in the igneous crust, z, and mass of liquid remaining, F, is given by $z = t_c F$ where t_c is the crustal thickness. This relationship is used to generate the right-hand scale in Figure 10, and also provides an estimate of the relationship between the crystallization temperature and depth, under the caveat that the MELTS run used in the calculation was an isobaric simulation. In the crustal column shown in Figure 10b, the 20 km of igneous material added is then composed of a lower 1.2 km of olivine-rich ultramafic cumulates, a lower and middle crust of gabbroic cumulates and an upper crust composed of dykes, sills and lavas [*Maclennan et al.*, 2001b]. This model matches the seismic discontinuity model from Figure 8, for the northern NVZ with discontinuity B corresponding to the seismic Moho, in this case the transition between high-velocity ultramafic cumulates and the lower velocity gabbroic crust.

The results of MELTS models run to reproduce key features of crustal structure in central Iceland are shown in Figures 10c,d. In this case the ~40 km thick crust is formed by solidification of equal proportions of depleted and enriched mantle melts. The differences in the crystallization behavior of the two mantle melt compositions is clear. The enriched melt hits its liquidus at 1348°C, a much higher temperature than the depleted melt. The temperature interval over which olivine-only crystallization occurs is also much larger, with plagioclase not joining the crystallizing assemblage until 1170°C when 20% of the original liquid mass has been lost to crystallization of ultramafic cumulates. If we assume a steady-state one-dimensional geotherm in the crust then it is possible to link the extent of crystallization, depth and temperature through the expressions $z = \overline{F} t_c$ and

$$\overline{F} = X_e F_e + (1 - X_e) F_d \tag{1}$$

where X_e is the mass proportion of melt supplied from the mantle that is enriched, F_e is the liquid fraction remaining of the enriched mantle melt at a given temperature and F_d is the equivalent for the depleted mantle melt at that temperature. The term $\overline{F}$ can then be cal-

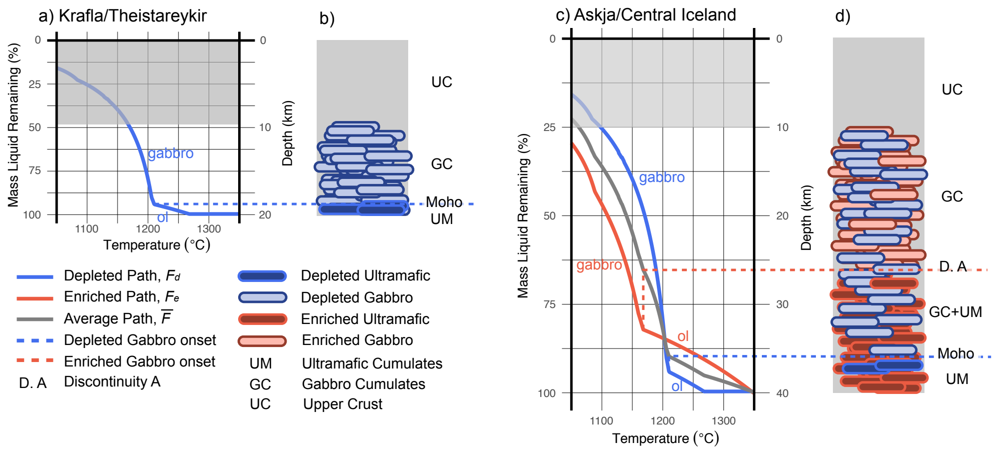

Figure 10. Petrological model linking mantle melt crystallization paths to crustal structure variation. See text for detailed explanation. a) MELTS model of fractional crystallization of a depleted mantle melt composition, showing the relationship between original liquid mass remaining and temperature (blue line). The parts of the crystallization path labeled 'ol' and 'gabbro' correspond to the segments where only olivine-rich ultramafic cumulates are generated by crystallization and those where cumulate gabbro is the solid product. The conversion to depth is shown on the right-hand axis, under the assumption of a pure stacked-sills model of accretion. The gray shaded zone corresponds to the upper crust. The total supplied melt thickness here is close to 20 km, and the dominance of depleted melts is designed to match the characteristics of the northern part of the NVZ at Krafla/Theistareykir. b) Sketch model of crustal structure generated by the crystallization model in (a). c) MELTS models of crystallization of depleted (blue) and enriched (red) mantle melts. The gray line shows the mean liquid fraction remaining, $\overline{F}$, which can be used to relate temperature to depth with a simple crustal accretion model. Dashed lines show the temperatures and depths at which depleted and enriched melts commence crystallization of gabbroic cumulates. The total supplied melt thickness is 40 km with equal proportions of depleted and enriched melts, designed to match the characteristics of the southern NVZ near Askja. d) Sketch model of resulting crustal structure.

culated as a function of temperature using the MELTS results for the depleted and enriched melts (blue and red curves in Figure 10c). In turn, it is then possible to relate temperature to depth in the crustal accretion model through $\overline{F}$. These relationships allow the prediction of the temperatures and depths at which certain solid cumulate rocks will be generated by crystallization from the enriched and depleted mantle melts. This crustal structure is depicted in Figure 10d. At temperatures higher than 1211°C, equivalent to a depth of 36 km, only olivine crystallizes from both enriched and depleted melts, creating a pile of ultramafic cumulates at the base of the igneous crust with seismic properties very similar to that of the mantle. At temperatures between 1211°C and 1170°C, depths of 26 and 36 km, corresponding to the interval between the red and blue dashed lines on Figures 10c,d, the depleted melt is crystallizing gabbroic cumulates, while the enriched melt is generating only olivine-rich ultramafic cumulates. This depth interval will therefore be composed of a mixture of gabbroic and ultramafic cumulates and will have a seismic velocity intermediate between that of the underlying mantle and the overlying gabbroic cumulates. It is proposed that this mixed layer corresponds to seismic layer B from Figure 8. At depths of less than 26 km both enriched and depleted melt are at sufficiently low temperatures to produce gabbroic cumulates: material with lower seismic velocities that could provide a suitable match to seismic layer A. The uppermost 10 km is once again proposed to be composed of variably fractured and altered lavas and small intrusions.

The density of olivine rich cumulates at their crystallization temperature is ≈3200 kg m^{-3}, and for gabbroic cumulates ≈2950 kg m^{-3}. Given the relative proportions of cumulates making up the lower layer (Figure 10d), this would give a mean density of ≈3000 kg m^{-3}; denser than typical oceanic crust. The suggestion of a denser lower-crust is supported by gravity studies of Iceland [*Darbyshire et al.*, 2000; *Kaban et al.*, 2002], though estimates of lower-crustal densities are slightly higher than suggested by our petrological model (≈3050-3100 kg m^{-3}). However as cumulate material cools below the crystallization temperature it will further increase in density, e.g. cooling from the crystallization temperature to 600°C, will increase the density to >3050 kg m^{-3}.

These simple petrological and crustal accretion models demonstrate that the variation in seismic discontinuity structure under the rift zones between the center of Iceland and the coasts can be understood as a consequence of the increased importance of the supply of deep, small degree, enriched mantle melts close to the plume center. The differing crystallization behavior of the enriched and depleted melts can generate the layered structure observed in central Iceland, with layer B corresponding to a depth and temperature interval where depleted melts are forming gabbroic cumulates, but enriched melts are only adding olivine-rich ultramafic cumulates to the solid crust.

5 Discussion

We observe a crustal velocity structure defined by an upper crust consisting of high velocity-gradients to depths of ~10 km underlain by either one or two major crustal discontinuities. Petrological modeling shows that structure can be explained by accounting for the variability in melt composition with distance from the plume center.

5.1 Upper crust

The high velocity-gradient upper crust is generally thought to consist of the unconsolidated lava pile and dyke intrusions. Closing of fractures under lithospheric pressure and increased mineral infilling by hydrothermal deposits reduces pore space with depth, explaining the rapidly increasing velocity with depth [*Flóvenz and Gunnarsson*, 1991]. The abrupt decrease in seismic velocity-gradient beneath depths of ~10 km is interpreted as a transition to consolidated rock.

5.2 Crustal thickness

Given the observation of two major discontinuities, if we wish to define crustal thickness, it is necessary to decide which of the imaged discontinuities to interpret as the seismic Moho. Debates on whether the Icelandic crust is thin or thick have been ongoing since the earliest measurements of crustal thickness. The observation of two seismic discontinuities representing sharp velocity increases provides a clear explanation as to why previous studies have diverged in their estimates of crustal thickness, since sharp seismic boundaries appear to exist at two different depths.

Using the nomenclature of previous studies, discontinuity A would be interpreted as the boundary between layers 3 and 4. Whether the underlying layer (layer B or 4) is interpreted as being part of the crust or of the mantle would then determine which of the imaged discontinuities would be thought to define crustal thickness. Recently opinions have converged to a prediction of a thick crust based on observations of gravity, surface wave dispersion, previous RF studies and refracted seismic phase arrivals [*Darbyshire et al.*, 2000;

Kaban et al., 2002; *Allen et al.*, 2002]. Results from our petrological modeling indicate that this deep layer is likely to consist of a combination of gabbroic and olivine-rich ultramafic cumulates. Thus if we base our decision on the general agreement of current literature, and the results of our own modeling, then the deeper layer B would be interpreted as being part of the lower crust with the discontinuity defining its base (i.e. discontinuity B) representing the seismic Moho.

Assuming this to be the case, we compare an extrapolated surface of discontinuity B to other recent crustal models in Figure 11. Our observations correlate well with the models of *Darbyshire et al.* [2000] (based on gravity measurements constrained by RFs and refraction study point estimates) and *Allen et al.* [2002] (based on surface wave dispersion measurements constrained by RFs and refraction study point estimates). Both our estimate, and previous models show increased crustal thickness in the Northwest Fjords and in Central and Eastern Iceland, with deepest Moho observations centered in the NW corner of Vatnajökull ice cap. We also agree on an abrupt step-like increase in crustal thickness moving southwards along the NVZ. Our observations require slightly thinner estimates of the maximum crustal thickness than previous studies. We improve our crustal thickness model by adding point constraints from refraction surveys (see Table S1 in Supplementary Material [*Staples et al.*, 1997; *Darbyshire et al.*, 1998; *Bjarnason et al.*, 1993; *Menke et al.*, 1998; *Weir et al.*, 2001]) (Figure 11b). This adds a large number of point constraints in SW Iceland where we have few other observations. However, the overall shape of the crustal thickness estimate is little changed, as additional point constraints are consistent with our observations (see Supplementary Figure S17 for a more detailed map of crustal thickness defined by this study).

The large crustal thicknesses beneath Vatnajökull ice cap have previously been linked to enhanced melting due to a combination of high mantle temperatures and active upwelling above the plume core [*Darbyshire et al.*, 2000], an interpretation which is supported by our petrological model. Plate reconstructions show a general WNW motion of the North Atlantic relative to the Iceland plume over the past 60 Ma, such that the plume tracks SE from the Northwest Fjords at 20−25Ma to its present location in central Iceland [*Vink*, 1984; *Lawver and Müller*, 1994; *Mihalffy et al.*, 2008]. This would explain observations of thickened crust beneath the Northwest Fjords, which may also have been formed close to the plume center in the past.

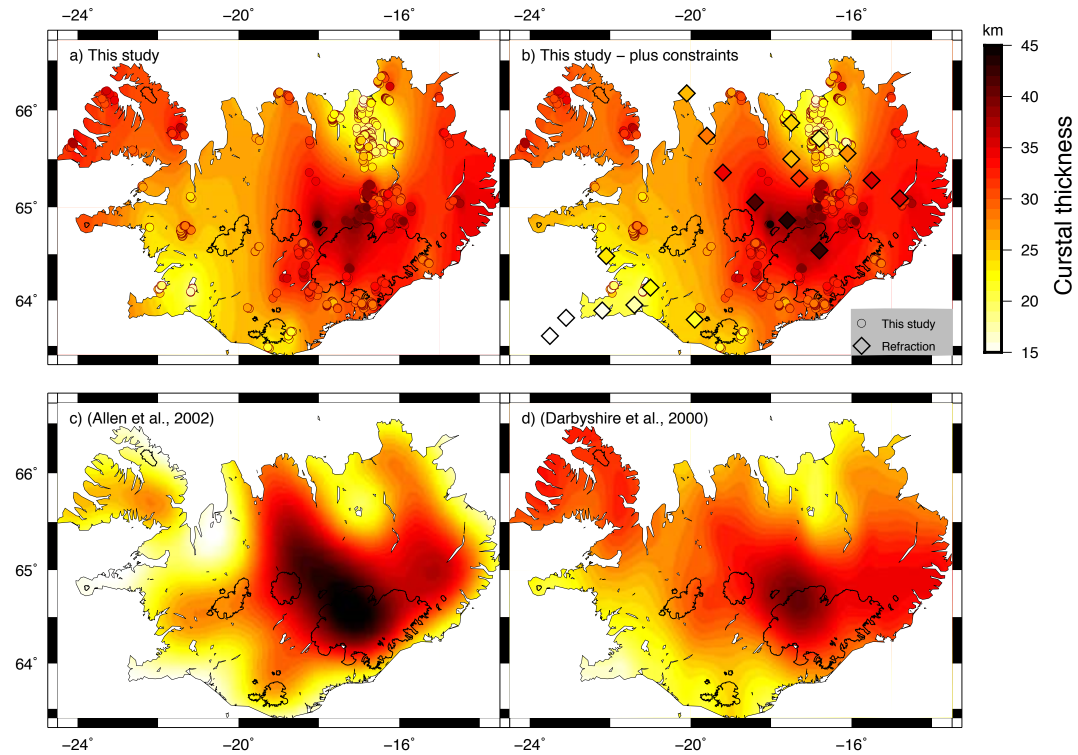

Figure 11. Estimates of crustal thickness based on **a**) the discontinuity B observations made in this study, **b**) the results of this study with added constraints from refraction studies, and the crustal models of **c**) [*Allen et al.*, 2002] and **d**) [*Darbyshire et al.*, 2000]. Data defining our final crustal thickness model (**b** and shown in Supplementary Figure S17) is uploaded as supporting material.

5.3 Potential causes of multi-layered crustal structure

Irrespective of which discontinuity is interpreted as the seismic Moho, we are left with the question of what the apparent two-stepped velocity structure represents physically, and how it has been formed. One explanation we have already explored with our petrologiocal model is that this feature is actively forming in the present day, caused by the variable nature of crustal production due to varying melt composition with distance from the plume center (as discussed in section 4). An alternative explanation is that discontinuity A represents a pre-existing ancient feature which interacts with current crustal formation in Central Iceland. We explore this hypothesis below.

5.3.1 Magmatic underplating or intrusion

It is possible that layer B could represent underplated or heavily intruded material, added to the bottom of pre-existing oceanic crust, such that the discontinuity A represents an ancient Moho. In this model, crust of near constant thickness (~20 km) is formed in normal spreading ridge conditions with an above average mantle temperature. The presence of the Icelandic plume beneath this region generates additional melt, which becomes trapped beneath the pre-existing crust. An eastwards jump in the location of active spreading (following the location of the plume), moves active spreading to this region.

If this model were correct, we might expect pre-existing oceanic crust to be stretched and thinned, as it is currently being rifted. While the exact chronology of rift migration is debated, the full spreading distances across the NVZ since the onset of active rifting is generally agreed to be on the order of ≈120 km [*Garcia et al.*, 2003; *Harðarson et al.*, 2008]. Assuming a pre-existing crust of 20 km thickness before the onset of rifting in the NVZ, and that rifting is distributed across a region equivalent to the present day width of the NVZ (~50 km), simple volume conservation calculations suggest that the ancient oceanic crust would have been thinned to ~8 km thickness over this period. However, active rifting also causes the addition of new melt intruded into the crust by decompression melting of the underlying mantle. Therefore thinning of the ancient crust could be offset by intrusion of new material. To maintain a thickness of 20 km after stretching this requires layer A to be made up of ~40% original ancient crust and ~60% newly intruded material. This is assuming that new material intruded into the pre-existing crust is of the same composition, which may not be the case with the addition of plume induced melting, as discussed in section 4.

We do not observe significant thinning of layer A (which would represent the ancient oceanic crust in this scenario) across present day active rift zones. In fact a thickening of layer A is observed towards the southern NVZ around Vatnajökull. Therefore for this interpretation to be viable, addition of new intruded igneous material into the upper crust must outweigh the effects of rift induced thinning. In this case, additional melt produced in the region directly overlying the mantle plume stem could produce greater intrusion of material into the crust above Vatnajökull, depressing the ancient Moho.

The process of magmatic underplating has been hypothesized to occur beneath numerous volcanic islands including Hawaii [*Watts et al.*, 1985; *Wolfe et al.*, 1994; *Leahy et al.*, 2010] the Marquesas Islands [*Caress et al.*, 1995; *McNutt and Bonneville*, 2000], Cook Islands, Society Islands and Line Islands [*Leahy and Park*, 2005] in the south Pacific, and the Canary islands [*Dañobeitia and Canales*, 2000] in the Atlantic. Underplating has also been cited as an explanation for observations of a two-layered discontinuity structure imaged in previous RF studies [*Leahy et al.*, 2010], and two observed reflectors in refraction studies [*Caress et al.*, 1995]. In these cases, velocity estimates of interpreted underplated material lie somewhere between standard lower oceanic crust and upper mantle [*Caress et al.*, 1995], consistent with estimates of Icelandic layer 4 (layer B) seismic velocities. However, these observations are on a much smaller scale than the layering we observe in Iceland, with typical underplating layer thickness ranging from 2-10 km; significantly less than the maximum 20 km thickness of Layer B. In addition, all of these studies are in intra-plate oceanic settings, quite different to the Icelandic setting where the underlying hotspot also interacts with a region of active rifting.

Our petrological modeling has shown it is possible to form the observed multi-layered discontinuity in the present day rifting, simply due to variability in melt composition along the region of active rifting. Given this simple explanation, as well the fact that layer A shows no thinning as predicted for an underplating model, we hypothesize that this present day formation hypothesis provides a more likely explanation for our observed structure. Regardless of the fact that other plume locations may well exhibit similar multi-stepped velocity structure due to an underplating cause, Iceland is in a significantly different setting. Given the interaction of active rifting and the underlying hotspot, and we would not expect Icelandic crust to be formed via the same processes as ocean island settings.

6 Conclusion

A joint inversion of RFs in combination with surface wave dispersion curves reveals the crustal velocity structure of Iceland.

The multi-layered crustal structure consists of: an upper crust showing rapidly increasing seismic velocity down to depths of 6-10 km, underlain by either one or two discontinuities (A and B). Discontinuity A is found throughout Iceland, with a near constant depth of 20 km. Discontinuity B shows great depth variability from 25-44 km and is only present in specific regions, defining the base of a lens-like lower layer with a maximum thickness beneath Vatnajökull ice cap.

The structure of the Icelandic crust has been a long running and controversial debate, with estimates of Icelandic crustal thickness ranging from a "thin" 20 km crust to a "thick" 40 km crust. The two major discontinuities observed in this study highlights how these two end member models have come about, as sharp increases in seismic velocity, either of which could be interpreted as the seismic Moho, can be found at both of these depths. We produce new maps of crustal thickness, defined as the depth to the deepest imaged discontinuity, which are consistent with other recent measurements.

We hypothesize that the observed multi-layered structure is a direct consequence of crust generated by ridge-plume interaction. We present two possible interpretations:

1. That the deeper layer represents underplated or heavily intruded plume derived magmatic material underlying a pre-existing oceanic crustal Moho, as has been suggested to occur in many other hotspot locations. However this explanation may not be valid in an plume-ridge interacting setting, as opposed to ocean island settings where it has been previously suggested to occur.
2. Alternatively the discontinuities represent bulk changes in crustal mineralogy caused by interaction of melts of varying composition, with lateral variability explained by the increase of deep enriched mantle melts with decreasing distance to the plume center. Petrological modeling is used to demonstrate that this interpretation is consistent with our observations, as well as erupted melt geochemistry along the actively rifting Northern Volcanic Zone.

Acknowledgments

Discontinuity observations reported, as well as the original receiver functions and dispersion curves analysed, can be accessed in the attached supplementary material. Please remember to cite the article when making use of any of the provided data. Seismometers were borrowed from the Natural Environment Research Council (NERC) SEIS-UK (loans 968 and 1022). We are grateful for research grants from the NERC and the European Community's Seventh Framework Program Grant No. 308377 (FUTUREVOLC). AD was funded by the European Research Council (ERC) under the European Union's Horizon 2020 research and innovation programme (grant agreement no. 681535 ATUNE) and a a Vici award number 016.160.310/526 from the Netherlands organization for scientific research (NWO). We thank Bryndís Brandsdóttir, Sveinbjórn Steinthórsson and all those who assisted with fieldwork in Iceland. Chris Bean (University College Dublin), the British Geological Survey and the Icelandic Meteorological Office (IMO) kindly provided additional data from their seismometers: data delivery from IMO seismic database 20141124/01 and 20151001/01. Dept. Earth Sciences, Cambridge contribution number ESC4074.

References

Akaike, H. (1974), A new look at the statistical model identification, *IEEE transactions on automatic control*, *19*(6), 716–723.

Allen, R. M., G. Nolet, W. J. Morgan, K. Vogfjörd, M. Nettles, G. Ekström, B. H. Bergsson, P. Erlendsson, G. Foulger, S. Jakobsdóttir, et al. (2002), Plume-driven plumbing and crustal formation in Iceland, *J. Geophys. Res.: Solid Earth*, *107*(B8).

Beblo, M., and A. Bjornsson (1980), Model of electrical-resistivity beneath NE Iceland, correlation with temperature, *Journal OF Geophysics-Zeitschrift Fur Geophysik*, *47*(1-3), 184–190.

Berteussen, K.-A. (1977), Moho depth determinations based on spectral-ratio analysis of NORSAR long-period P waves, *Phys. Earth Planet. Inter.*, *15*(1), 13–27.

Bjarnason, I. T., W. Menke, Ó. G. Flóvenz, and D. Caress (1993), Tomographic image of the mid-Atlantic plate boundary in southwestern Iceland, *J. Geophys. Res.: Solid Earth*, *98*(B4), 6607–6622.

Bjarnason, I. T., C. J. Wolfe, S. C. Solomon, and G. Gudmundson (1996), Initial results from the ICEMELT experiment: Body-wave delay times and shear-wave splitting across Iceland, *Geophys. Res. Lett.*, *23*(5), 459–462.

Brandsdóttir, B., and W. H. Menke (2008), The seismic structure of Iceland, *Jökull*, *58*(17–34).

Brandsdóttir, B., W. Menke, P. Einarsson, R. S. White, and R. K. Staples (1997), Färoe-Iceland ridge experiment 2. crustal structure of the Krafla central volcano, *J. Geophys. Res.: Solid Earth*, *102*(B4), 7867–7886.

Caress, D. W., M. K. McNutt, R. S. Detrick, and J. C. Mutter (1995), Seismic imaging of hotspot-related crustal underplating beneath the Marquesas islands, *Nature*, *373*(6515), 600–603.

Carlson, R., and C. Herrick (1990), Densities and porosities in the oceanic crust and their variations with depth and age, *J. Geophys. Res.: Solid Earth*, *95*(B6), 9153–9170.

Dañobeitia, J., and J. Canales (2000), Magmatic underplating in the Canary Archipelago, *J. Volcanol. Geoth. Res.*, *103*(1), 27–41.

Danyushevsky, L. V., and P. Plechov (2011), Petrolog3: Integrated software for modeling crystallization processes, *Geochemistry, Geophysics, Geosystems*, *12*(7).

Darbyshire, F. A., I. T. Bjarnason, R. S. White, and Ó. G. Flóvenz (1998), Crustal structure above the Iceland mantle plume imaged by the ICEMELT refraction profile, *Geophys. J. Int.*, *135*(3), 1131–1149.

Darbyshire, F. A., R. S. White, and K. F. Priestley (2000), Structure of the crust and uppermost mantle of Iceland from a combined seismic and gravity study, *Earth Planet. Sci. Lett.*, *181*(3), 409–428.

DeMets, C., R. G. Gordon, and D. F. Argus (2010), Geologically current plate motions, *Geophys. J. Int.*, *181*(1), 1–80.

Dueker, K. G., and A. F. Sheehan (1997), Mantle discontinuity structure from midpoint stacks of converted P to S waves across the Yellowstone hotspot track, *J. Geophys. Res.*, *102*, 8313–8327.

Einarsson, P. (2008), Plate boundaries, rifts and transforms in Iceland, *Jökull*, *58*(12), 35–58.

Eysteinsson, H., and J. F. Hermance (1985), Magnetotelluric measurements across the eastern neovolcanic zone in south Iceland, *J. Geophys. Res.: Solid Earth*, *90*(B12), 10,093–10,103.

Flóvenz, Ó. G., and K. Gunnarsson (1991), Seismic crustal structure in Iceland and surrounding area, *Tectonophysics*, *189*(1), 1–17.

Flóvenz, Ó. G., and K. Saemundsson (1993), Heat flow and geothermal processes in Iceland, *Tectonophysics*, *225*(1-2), 123–138.

Foulger, G., M. Pritchard, B. Julian, J. Evans, R. Allen, G. Nolet, W. Morgan, B. Bergsson, P. Erlendsson, S. Jakobsdottir, et al. (2000), The seismic anomaly beneath Iceland extends down to the mantle transition zone and no deeper, *Geophys. J. Int.*, *142*(3), F1–F5.

French, S. W., and B. Romanowicz (2015), Broad plumes rooted at the base of the Earth's mantle beneath major hotspots, *Nature*, *525*(7567), 95–99.

Garcia, S., N. O. Arnaud, J. Angelier, F. Bergerat, and C. Homberg (2003), Rift jump process in northern Iceland since 10 ma from ^{40}Ar/^{39}Ar geochronology, *Earth Planet. Sci. Lett.*, *214*(3), 529–544.

Gebrande, H., H. Miller, and P. Einarsson (1980), Seismic structure of Iceland along RRISP-profile-I, *Journal of Geophysics-Zeitschrift Fur Geophysik*, *47*(1-3), 239–249.

Ghiorso, M. S., and R. O. Sack (1995), Chemical mass transfer in magmatic processes IV. a revised and internally consistent thermodynamic model for the interpolation and extrapolation of liquid−solid equilibria in magmatic systems at elevated temperatures and pressures, *Contributions to Mineralogy and Petrology*, *119*(2-3), 197–212.

Green, R. G., K. F. Priestley, and R. S. White (2017), Ambient noise tomography reveals upper crustal structure of Icelandic rifts, *Earth Planet. Sci. Lett.*.

Gudmundsson, A. (2000), Dynamics of volcanic systems in Iceland: example of tectonism and volcanism at juxtaposed hot spot and mid-ocean ridge systems, *Ann. Rev. Earth Planet Sci.*, *28*(1), 107–140.

Harðarson, B. S., J. G. Fitton, and Á. Hjartarson (2008), Tertiary volcanism in Iceland, *Jökull*, *58*, 161–178.

Harmon, N., and C. A. Rychert (2016), Joint inversion of teleseismic and ambient noise rayleigh waves for phase velocity maps, an application to iceland, *Journal of Geophysical Research: Solid Earth*, *121*(8), 5966–5987.

Herrmann, R. B. (2013), Computer programs in seismology: An evolving tool for instruction and research, *Seismological Research Letters*, *84*(6), 1081–1088.

Hersir, G. P., A. Björnsson, and L. B. Pedersen (1984), Magnetotelluric survey across the active spreading zone in southwest Iceland, *J. Volcanol. Geoth. Res.*, *20*(3-4), 253–265.

Jenkins, J., S. Cottaar, R. White, and A. Deuss (2016), Depressed mantle discontinuities beneath Iceland: Evidence of a garnet controlled 660 km discontinuity?, *Earth Planet. Sci. Lett.*, *433*, 159–168.

Julia, J., C. Ammon, R. Herrmann, and A. M. Correig (2000), Joint inversion of receiver function and surface wave dispersion observations, *Geophys. J. Int.*, *143*(1), 99–112.

Kaban, M. K., Ó. G. Flóvenz, and G. Pálmason (2002), Nature of the crust-mantle transition zone and the thermal state of the upper mantle beneath Iceland from gravity modelling, *Geophys. J. Int.*, *149*(2), 281–299.

Kelemen, P. B., K. Koga, and N. Shimizu (1997), Geochemistry of gabbro sills in the crust-mantle transition zone of the oman ophiolite: Implications for the origin of the oceanic lower crust, *Earth and Planetary Science Letters*, *146*(3-4), 475–488.

Kind, R., X. Yuan, J. Saul, D. Nelson, S. Sobolev, J. Mechie, W. Zhao, G. Kosarev, J. Ni, U. Achauer, et al. (2002), Seismic images of crust and upper mantle beneath tibet: evidence for eurasian plate subduction, *Science*, *298*(5596), 1219–1221.

Lawver, L. A., and R. D. Müller (1994), Iceland hotspot track, *Geology*, *22*(4), 311–314.

Leahy, G. M., and J. Park (2005), Hunting for oceanic island Moho, *Geophys. J. Int.*, *160*(3), 1020–1026.

Leahy, G. M., J. A. Collins, C. J. Wolfe, G. Laske, and S. C. Solomon (2010), Underplating of the Hawaiian swell: evidence from teleseismic receiver functions, *Geophys. J. Int.*, *183*(1), 313–329.

Lekic, V., S. W. French, and K. M. Fischer (2011), Lithospheric thinning beneath rifted regions of Southern California, *Science*, *334*(6057), 783–787.

Ligorría, J. P., and C. J. Ammon (1999), Iterative deconvolution and receiver-function estimation, *Geol. Soc. Am. Bull.*, *89*(5), 1395–1400.

Maclennan, J. (2008a), Lead isotope variability in olivine-hosted melt inclusions from Iceland, *Geochimica et Cosmochimica Acta*, *72*(16), 4159–4176.

Maclennan, J. (2008b), Concurrent mixing and cooling of melts under iceland, *Journal of Petrology*, *49*(11), 1931–1953.

Maclennan, J., D. McKenzie, and K. Gronvöld (2001a), Plume-driven upwelling under central Iceland, *Earth Planet. Sci. Lett.*, *194*(1), 67–82.

Maclennan, J., D. McKenzie, K. Gronvöld, and L. Slater (2001b), Crustal accretion under northern Iceland, *Earth Planet. Sci. Lett.*, *191*(3), 295–310.

McNutt, M., and A. Bonneville (2000), A shallow, chemical origin for the Marquesas swell, *Geophys. Geochem. Geosys.*, *1*(6).

Menke, W., and V. Levin (1994), Cold crust in a hot spot, *Geophys. Res. Lett.*, *21*(18), 1967–1970.

Menke, W., and D. Sparks (1995), Crustal accretion model for Iceland predicts âĂŸ-coldâĂŹcrust, *Geophys. Res. Lett.*, *22*(13), 1673–1676.

Menke, W., B. Brandsdóttir, P. Einarsson, and I. T. Bjarnason (1996), Reinterpretation of the RRISP-77 Iceland shear-wave profiles, *Geophys. J. Int.*, *126*(1), 166–172.

Menke, W., M. West, B. Brandsdóttir, and D. Sparks (1998), Compressional and shear velocity structure of the lithosphere in northern Iceland, *Geol. Soc. Am. Bull.*, *88*(6), 1561–1571.

Mihalffy, P., B. Steinberger, and H. Schmeling (2008), The effect of the large-scale mantle flow field on the Iceland hotspot track, *Tectonophysics*, *447*(1), 5–18.

Nábělek, J., G. Hetényi, J. Vergne, S. Sapkota, B. Kafle, M. Jiang, H. Su, J. Chen, B.-S. Huang, et al. (2009), Underplating in the himalaya-tibet collision zone revealed by the hi-climb experiment, *Science*, *325*(5946), 1371–1374.

Pálmason, G. (1971), *Crustal structure of Iceland from explosion seismology*, vol. 40, Prentsmiðjan Leiftur.

Rudge, J. F., J. Maclennan, and A. Stracke (2013), The geochemical consequences of mixing melts from a heterogeneous mantle, *Geochimica et Cosmochimica Acta*, *114*, 112–143.

Saemundsson, K. (1974), Evolution of the axial rifting zone in northern Iceland and the Tjörnes fracture zone, *Geological Society of America Bulletin*, *85*(4), 495–504.

Schlindwein, V. (2006), On the use of teleseismic receiver functions for studying the crustal structure of Iceland, *Geophys. J. Int.*, *164*(3), 551–568.

Shorttle, O., and J. Maclennan (2011), Compositional trends of Icelandic basalts: Implications for short–length scale lithological heterogeneity in mantle plumes, *Geophys. Geochem. Geosys.*, *12*(11).

Shorttle, O., J. Maclennan, and S. Jones (2010), Control of the symmetry of plume-ridge interaction by spreading ridge geometry, *Geophys. Geochem. Geosys.*, *11*(7).

Shorttle, O., J. F. Rudge, J. Maclennan, and K. H. Rubin (2016), A statistical description of concurrent mixing and crystallization during morb differentiation: implications for trace element enrichment, *Journal of Petrology*, *57*(11-12), 2127–2162.

Slater, L., D. McKenzie, K. Grönvold, and N. Shimizu (2001), Melt generation and movement beneath Theistareykir, NE Iceland, *Journal of Petrology*, *42*(2), 321–354.

Smith, P. M., and P. D. Asimow (2005), Adiabat_1ph: A new public front-end to the MELTS, pMELTS, and pHMELTS models, *Geochemistry, Geophysics, Geosystems*, *6*(2).

Staples, R. K., R. S. White, B. Brandsdóttir, W. Menke, P. K. Maguire, and J. H. McBride (1997), Färoe-Iceland ridge experiment 1. crustal structure of northeastern Iceland, *J. Geophys. Res.: Solid Earth*, *102*(B4), 7849–7866.

Stefánsson, R., R. Böđvarsson, R. Slunga, P. Einarsson, S. Jakobsdóttir, H. Bungum, S. Gregersen, J. Havskov, J. Hjelme, and H. Korhonen (1993), Earthquake prediction research in the south Iceland seismic zone and the SIL project, *Geol. Soc. Am. Bull.*, *83*(3), 696–716.

Tauzin, B., T. Bodin, E. Debayle, J.-P. Perrillat, and B. Reynard (2016), Multi-mode conversion imaging of the subducted Gorda and Juan de Fuca plates below the North American continent, *Earth Planet. Sci. Lett.*, *440*, 135–146.

Vink, G. E. (1984), A hotspot model for iceland and the vøring plateau, *Journal of Geophysical Research: Solid Earth*, *89*(B12), 9949–9959.

Watts, A., U. Ten Brink, P. Buhl, and T. Brocher (1985), A multichannel seismic study of lithospheric flexure across the Hawaiian–Emperor seamount chain, *Nature*, *315*(6015), 105–111.

Weir, N. R., R. S. White, B. Brandsdóttir, P. Einarsson, H. Shimamura, and H. Shiobara (2001), Crustal structure of the northern Reykjanes Ridge and Reykjanes peninsula, southwest Iceland, *J. Geophys. Res.: Solid Earth*, *106*(B4), 6347–6368.

White, R., and D. McKenzie (1989), Magmatism at rift zones: the generation of volcanic continental margins and flood basalts, *J. Geophys. Res.: Solid Earth (1978–2012)*, *94*(B6), 7685–7729.

White, R. S. (1997), Rift–plume interaction in the north atlantic, *Philosophical Transactions of the Royal Society of London A: Mathematical, Physical and Engineering Sciences*, *355*(1723), 319–339.

Winpenny, B., and J. Maclennan (2011), A partial record of mixing of mantle melts preserved in Icelandic phenocrysts, *Journal of Petrology*, *52*(9), 1791–1812.

Wolfe, C. J., M. K. McNutt, and R. S. Detrick (1994), The Marquesas archipelagic apron: Seismic stratigraphy and implications for volcano growth, mass wasting, and crustal underplating, *J. Geophys. Res.: Solid Earth*, *99*(B7), 13,591–13,608.

References

Akaike, H. (1974), A new look at the statistical model identification, *IEEE transactions on automatic control*, *19*(6), 716–723.

Allen, R. M., G. Nolet, W. J. Morgan, K. Vogfjörd, M. Nettles, G. Ekström, B. H. Bergsson, P. Erlendsson, G. Foulger, S. Jakobsdóttir, et al. (2002), Plume-driven plumbing and crustal formation in Iceland, *J. Geophys. Res.: Solid Earth*, *107*(B8).

Beblo, M., and A. Bjornsson (1980), Model of electrical-resistivity beneath NE Iceland, correlation with temperature, *Journal OF Geophysics-Zeitschrift Fur Geophysik*, *47*(1-3), 184–190.

Berteussen, K.-A. (1977), Moho depth determinations based on spectral-ratio analysis of NORSAR long-period P waves, *Phys. Earth Planet. Inter.*, *15*(1), 13–27.

Bjarnason, I. T., W. Menke, Ó. G. Flóvenz, and D. Caress (1993), Tomographic image of the mid-Atlantic plate boundary in southwestern Iceland, *J. Geophys. Res.: Solid Earth*, *98*(B4), 6607–6622.

Bjarnason, I. T., C. J. Wolfe, S. C. Solomon, and G. Gudmundson (1996), Initial results from the ICEMELT experiment: Body-wave delay times and shear-wave splitting across Iceland, *Geophys. Res. Lett.*, *23*(5), 459–462.

Brandsdóttir, B., and W. H. Menke (2008), The seismic structure of Iceland, *Jökull*, *58*(17–34).

Brandsdóttir, B., W. Menke, P. Einarsson, R. S. White, and R. K. Staples (1997), Färoe-Iceland ridge experiment 2. crustal structure of the Krafla central volcano, *J. Geophys. Res.: Solid Earth*, *102*(B4), 7867–7886.

Caress, D. W., M. K. McNutt, R. S. Detrick, and J. C. Mutter (1995), Seismic imaging of hotspot-related crustal underplating beneath the Marquesas islands, *Nature*, *373*(6515), 600–603.

Carlson, R., and C. Herrick (1990), Densities and porosities in the oceanic crust and their variations with depth and age, *J. Geophys. Res.: Solid Earth*, *95*(B6), 9153–9170.

Dañobeitia, J., and J. Canales (2000), Magmatic underplating in the Canary Archipelago, *J. Volcanol. Geoth. Res.*, *103*(1), 27–41.

Danyushevsky, L. V., and P. Plechov (2011), Petrolog3: Integrated software for modeling crystallization processes, *Geochemistry, Geophysics, Geosystems*, *12*(7).

Darbyshire, F. A., I. T. Bjarnason, R. S. White, and Ó. G. Flóvenz (1998), Crustal structure above the Iceland mantle plume imaged by the ICEMELT refraction profile, *Geophys. J. Int.*, *135*(3), 1131–1149.

Darbyshire, F. A., R. S. White, and K. F. Priestley (2000), Structure of the crust and uppermost mantle of Iceland from a combined seismic and gravity study, *Earth Planet. Sci. Lett.*, *181*(3), 409–428.

DeMets, C., R. G. Gordon, and D. F. Argus (2010), Geologically current plate motions, *Geophys. J. Int.*, *181*(1), 1–80.

Dueker, K. G., and A. F. Sheehan (1997), Mantle discontinuity structure from midpoint stacks of converted P to S waves across the Yellowstone hotspot track, *J. Geophys. Res.*, *102*, 8313–8327.

Einarsson, P. (2008), Plate boundaries, rifts and transforms in Iceland, *Jökull*, *58*(12), 35–58.

Eysteinsson, H., and J. F. Hermance (1985), Magnetotelluric measurements across the eastern neovolcanic zone in south Iceland, *J. Geophys. Res.: Solid Earth*, *90*(B12), 10,093–10,103.

Flóvenz, Ó. G., and K. Gunnarsson (1991), Seismic crustal structure in Iceland and surrounding area, *Tectonophysics*, *189*(1), 1–17.

Flóvenz, Ó. G., and K. Saemundsson (1993), Heat flow and geothermal processes in Iceland, *Tectonophysics*, *225*(1-2), 123–138.

Foulger, G., M. Pritchard, B. Julian, J. Evans, R. Allen, G. Nolet, W. Morgan, B. Bergsson, P. Erlendsson, S. Jakobsdottir, et al. (2000), The seismic anomaly beneath Iceland extends down to the mantle transition zone and no deeper, *Geophys. J. Int.*, *142*(3), F1–F5.

French, S. W., and B. Romanowicz (2015), Broad plumes rooted at the base of the Earth's mantle beneath major hotspots, *Nature*, *525*(7567), 95–99.

Garcia, S., N. O. Arnaud, J. Angelier, F. Bergerat, and C. Homberg (2003), Rift jump process in northern Iceland since 10 ma from ^{40}Ar/^{39}Ar geochronology, *Earth Planet. Sci. Lett.*, *214*(3), 529–544.

Gebrande, H., H. Miller, and P. Einarsson (1980), Seismic structure of Iceland along RRISP-profile-I, *Journal of Geophysics-Zeitschrift Fur Geophysik*, *47*(1-3), 239–249.

Ghiorso, M. S., and R. O. Sack (1995), Chemical mass transfer in magmatic processes IV. a revised and internally consistent thermodynamic model for the interpolation and extrapolation of liquid−solid equilibria in magmatic systems at elevated temperatures and pressures, *Contributions to Mineralogy and Petrology*, *119*(2-3), 197–212.

Green, R. G., K. F. Priestley, and R. S. White (2017), Ambient noise tomography reveals upper crustal structure of Icelandic rifts, *Earth Planet. Sci. Lett.*.

Gudmundsson, A. (2000), Dynamics of volcanic systems in Iceland: example of tectonism and volcanism at juxtaposed hot spot and mid-ocean ridge systems, *Ann. Rev. Earth Planet Sci.*, *28*(1), 107–140.

Harðarson, B. S., J. G. Fitton, and Á. Hjartarson (2008), Tertiary volcanism in Iceland, *Jökull*, *58*, 161–178.

Harmon, N., and C. A. Rychert (2016), Joint inversion of teleseismic and ambient noise rayleigh waves for phase velocity maps, an application to iceland, *Journal of Geophysical Research: Solid Earth*, *121*(8), 5966–5987.

Herrmann, R. B. (2013), Computer programs in seismology: An evolving tool for instruction and research, *Seismological Research Letters*, *84*(6), 1081–1088.

Hersir, G. P., A. Björnsson, and L. B. Pedersen (1984), Magnetotelluric survey across the active spreading zone in southwest Iceland, *J. Volcanol. Geoth. Res.*, *20*(3-4), 253–265.

Jenkins, J., S. Cottaar, R. White, and A. Deuss (2016), Depressed mantle discontinuities beneath Iceland: Evidence of a garnet controlled 660 km discontinuity?, *Earth Planet. Sci. Lett.*, *433*, 159–168.

Julia, J., C. Ammon, R. Herrmann, and A. M. Correig (2000), Joint inversion of receiver function and surface wave dispersion observations, *Geophys. J. Int.*, *143*(1), 99–112.

Kaban, M. K., Ó. G. Flóvenz, and G. Pálmason (2002), Nature of the crust-mantle transition zone and the thermal state of the upper mantle beneath Iceland from gravity modelling, *Geophys. J. Int.*, *149*(2), 281–299.

Kelemen, P. B., K. Koga, and N. Shimizu (1997), Geochemistry of gabbro sills in the crust-mantle transition zone of the oman ophiolite: Implications for the origin of the oceanic lower crust, *Earth and Planetary Science Letters*, *146*(3-4), 475–488.

Kind, R., X. Yuan, J. Saul, D. Nelson, S. Sobolev, J. Mechie, W. Zhao, G. Kosarev, J. Ni, U. Achauer, et al. (2002), Seismic images of crust and upper mantle beneath tibet: evidence for eurasian plate subduction, *Science*, *298*(5596), 1219–1221.

Lawver, L. A., and R. D. Müller (1994), Iceland hotspot track, *Geology*, *22*(4), 311–314.

Leahy, G. M., and J. Park (2005), Hunting for oceanic island Moho, *Geophys. J. Int.*, *160*(3), 1020–1026.

Leahy, G. M., J. A. Collins, C. J. Wolfe, G. Laske, and S. C. Solomon (2010), Underplating of the Hawaiian swell: evidence from teleseismic receiver functions, *Geophys. J. Int.*, *183*(1), 313–329.

Lekic, V., S. W. French, and K. M. Fischer (2011), Lithospheric thinning beneath rifted regions of Southern California, *Science*, *334*(6057), 783–787.

Ligorría, J. P., and C. J. Ammon (1999), Iterative deconvolution and receiver-function estimation, *Geol. Soc. Am. Bull.*, *89*(5), 1395–1400.

Maclennan, J. (2008), Lead isotope variability in olivine-hosted melt inclusions from Iceland, *Geochimica et Cosmochimica Acta*, *72*(16), 4159–4176.

Maclennan, J., D. McKenzie, and K. Gronvöld (2001a), Plume-driven upwelling under central Iceland, *Earth Planet. Sci. Lett.*, *194*(1), 67–82.

Maclennan, J., D. McKenzie, K. Gronvöld, and L. Slater (2001b), Crustal accretion under northern Iceland, *Earth Planet. Sci. Lett.*, *191*(3), 295–310.

McNutt, M., and A. Bonneville (2000), A shallow, chemical origin for the Marquesas swell, *Geophys. Geochem. Geosys.*, *1*(6).

Menke, W., and V. Levin (1994), Cold crust in a hot spot, *Geophys. Res. Lett.*, *21*(18), 1967–1970.

Menke, W., and D. Sparks (1995), Crustal accretion model for Iceland predicts âĂŸ-coldâĂŹcrust, *Geophys. Res. Lett.*, *22*(13), 1673–1676.

Menke, W., B. Brandsdóttir, P. Einarsson, and I. T. Bjarnason (1996), Reinterpretation of the RRISP-77 Iceland shear-wave profiles, *Geophys. J. Int.*, *126*(1), 166–172.

Menke, W., M. West, B. Brandsdóttir, and D. Sparks (1998), Compressional and shear velocity structure of the lithosphere in northern Iceland, *Geol. Soc. Am. Bull.*, *88*(6), 1561–

1571.

Mihalffy, P., B. Steinberger, and H. Schmeling (2008), The effect of the large-scale mantle flow field on the Iceland hotspot track, *Tectonophysics*, *447*(1), 5–18.

Nábělek, J., G. Hetényi, J. Vergne, S. Sapkota, B. Kafle, M. Jiang, H. Su, J. Chen, B.-S. Huang, et al. (2009), Underplating in the himalaya-tibet collision zone revealed by the hi-climb experiment, *Science*, *325*(5946), 1371–1374.

Pálmason, G. (1971), *Crustal structure of Iceland from explosion seismology*, vol. 40, Prentsmiðjan Leiftur.

Rudge, J. F., J. Maclennan, and A. Stracke (2013), The geochemical consequences of mixing melts from a heterogeneous mantle, *Geochimica et Cosmochimica Acta*, *114*, 112–143.

Saemundsson, K. (1974), Evolution of the axial rifting zone in northern Iceland and the Tjörnes fracture zone, *Geological Society of America Bulletin*, *85*(4), 495–504.

Schlindwein, V. (2006), On the use of teleseismic receiver functions for studying the crustal structure of Iceland, *Geophys. J. Int.*, *164*(3), 551–568.

Shorttle, O., and J. Maclennan (2011), Compositional trends of Icelandic basalts: Implications for short–length scale lithological heterogeneity in mantle plumes, *Geophys. Geochem. Geosys.*, *12*(11).

Shorttle, O., J. Maclennan, and S. Jones (2010), Control of the symmetry of plume-ridge interaction by spreading ridge geometry, *Geophys. Geochem. Geosys.*, *11*(7).

Slater, L., D. McKenzie, K. Grönvold, and N. Shimizu (2001), Melt generation and movement beneath Theistareykir, NE Iceland, *Journal of Petrology*, *42*(2), 321–354.

Smith, P. M., and P. D. Asimow (2005), Adiabat_1ph: A new public front-end to the MELTS, pMELTS, and pHMELTS models, *Geochemistry, Geophysics, Geosystems*, *6*(2).

Staples, R. K., R. S. White, B. Brandsdóttir, W. Menke, P. K. Maguire, and J. H. McBride (1997), Färoe-Iceland ridge experiment 1. crustal structure of northeastern Iceland, *J. Geophys. Res.: Solid Earth*, *102*(B4), 7849–7866.

Stefánsson, R., R. Böđvarsson, R. Slunga, P. Einarsson, S. Jakobsdóttir, H. Bungum, S. Gregersen, J. Havskov, J. Hjelme, and H. Korhonen (1993), Earthquake prediction research in the south Iceland seismic zone and the SIL project, *Geol. Soc. Am. Bull.*, *83*(3), 696–716.

Tauzin, B., T. Bodin, E. Debayle, J.-P. Perrillat, and B. Reynard (2016), Multi-mode conversion imaging of the subducted Gorda and Juan de Fuca plates below the North American continent, *Earth Planet. Sci. Lett.*, *440*, 135–146.

Vink, G. E. (1984), A hotspot model for iceland and the vøring plateau, *Journal of Geophysical Research: Solid Earth*, *89*(B12), 9949–9959.

Watts, A., U. Ten Brink, P. Buhl, and T. Brocher (1985), A multichannel seismic study of lithospheric flexure across the Hawaiian–Emperor seamount chain, *Nature*, *315*(6015), 105–111.

Weir, N. R., R. S. White, B. Brandsdóttir, P. Einarsson, H. Shimamura, and H. Shiobara (2001), Crustal structure of the northern Reykjanes Ridge and Reykjanes peninsula, southwest Iceland, *J. Geophys. Res.: Solid Earth*, *106*(B4), 6347–6368.

White, R., and D. McKenzie (1989), Magmatism at rift zones: the generation of volcanic continental margins and flood basalts, *J. Geophys. Res.: Solid Earth (1978–2012)*, *94*(B6), 7685–7729.

White, R. S. (1997), Rift–plume interaction in the north atlantic, *Philosophical Transactions of the Royal Society of London A: Mathematical, Physical and Engineering Sciences*, *355*(1723), 319–339.

Winpenny, B., and J. Maclennan (2011), A partial record of mixing of mantle melts preserved in Icelandic phenocrysts, *Journal of Petrology*, *52*(9), 1791–1812.

Wolfe, C. J., M. K. McNutt, and R. S. Detrick (1994), The Marquesas archipelagic apron: Seismic stratigraphy and implications for volcano growth, mass wasting, and crustal underplating, *J. Geophys. Res.: Solid Earth*, *99*(B7), 13,591–13,608.